ELSEVIER

Journal of Nuclear Materials 265 (1999) 78–90

journal of nuclear materials

Effect of neutron flux on low temperature irradiation embrittlement of reactor pressure vessel steel

K. Dohi [a,*], T. Onchi [a], F. Kano [b], K. Fukuya [b], M. Narui [c], H. Kayano [c]

[a] *Central Research Institute of Electric Power Industry (CRIEPI), Komae Research Laboratory, 2-11-1, Iwado Kita, Komae-shi, Tokyo 201-8511, Japan*

[b] *Toshiba Corporation, Nuclear Engineering Laboratory, 4-1, Ukishima-cho, Kawasaki-ku, Kawasaki 210-0862, Japan*

[c] *The Oarai Branch, Institute for Materials Research, Tohoku University, Narita-cho, Oarai-machi, Ibaraki-ken 311-1313, Japan*

Received 24 March 1998; accepted 22 September 1998

Abstract

Miniature Charpy V-notch impact test specimens of commercial reactor pressure vessel (RPV) steels having high and low copper contents were irradiated at the different irradiation positions with neutron flux levels of $\sim 6 \times 10^{14}$, $\sim 7 \times 10^{15}$, and $\sim 8 \times 10^{16}$ n m^{-2} s^{-1} ($E > 1$ MeV) to fluence levels ranging from $\sim 6 \times 10^{21}$ to $\sim 7 \times 10^{22}$ n m^{-2} ($E > 1$ MeV) at temperatures of about 50°C to 150°C in the Japan Materials Testing Reactor (JMTR). The results showed that the radiation-induced increases in ductile-to-brittle transition temperature (ΔDBTT) at a neutron flux level of $\sim 6 \times 10^{14}$ n m^{-2}s^{-1} were greater than those for neutron flux level of $\sim 7 \times 10^{15}$ n m^{-2} s^{-1}. The neutron flux effect on embrittlement tended to be more pronounced in the lower neutron fluence range of $\sim 6 \times 10^{21}$–$\sim 1 \times 10^{22}$ n m^{-2} than in the higher fluence level of $\sim 7 \times 10^{22}$ n m^{-2}, and also to be larger for the low copper steel than for the high copper steel, although the ΔDBTT for the high copper steel was larger than that for the low copper steel regardless of neutron fluence or flux. The displacement dose rate effect identified by the data converted to the ΔDBTT for the full size Charpy specimens from those for the miniature Charpy specimens was consistent with that based on the comparison of the results in the literature.

PACS: 61.80.Hg; 81.40.Np; 81.70.Bt; 28.50.Dr

1. Introduction

Neutron irradiation of the reactor pressure vessel (RPV) in the beltline region causes localized accumulation of damage to the RPV steel, leading to RPV embrittlement and consequently to RPV integrity issues during normal and abnormal operating conditions. Since the solution of the integrity issues are closely linked with the embrittlement trend equation, a reliable prediction of plant life necessitates more accurate RPV embrittlement trend equation. Current trend equations such as USNRC R.G. 1.99, Rev. 2 [1] and the Japanese trend equation [2] are expressed as a function of chemistry factor calculated from the initial amounts of residual impurity elements like copper, phosphorus, silicon, and others, and of neutron fluence usually defined by the number of neutron having a high energy of more than 1 MeV(or 0.1 MeV). These expressions are based upon a statistical analysis of surveillance specimens data of commercial power reactors from pressurized water reactor (PWR) and boiling water reactor (BWR), which mean that the accuracy of this method inherently depends on the amount of data on surveillance specimens from commercial power reactors. For more advanced prediction of embrittlement, the trend equation must be based on the mechanistic understanding of RPV embrittlement.

Recent studies apparently show that irradiation embrittlement of RPV steels is affected not only by neutron fluence but also by other irradiation parameters like

* Corresponding author. Tel.: +81-33480 2111; fax: +81-33480 1668; e-mail: dohi@criepi.denken.or.jp

0022-3115/99/$ – see front matter
PII: S0022-3115(98)00611-4

neutron flux, neutron energy spectrum, gamma ray flux and so on. Neutron flux, in particular, appears to play an important role in 'accelerated' embrittlement of RPV steels at lower neutron fluences since the results of Charpy V-notch surveillance testing of ferritic steels from the High Flux Isotope Reactor (HFIR) pressure vessel irradiated at around 50°C were presented and discussed [3,4], although changes in neutron energy spectrum accompanied by lowering neutron flux and effects of gamma-induced displacements may be also involved with [5]. Lots of works on the effects of neutron flux on embrittlement of RPV steels have been conducted at an operating power reactor temperature of around 290°C and at different types of reactor [6–11]. Most of the results showed that the radiation-induced embrittlement of the steels were greater at lower neutron fluxes corresponding to power reactors than at higher fluxes corresponding to test reactors [6–9]. In contrast, few works have been done in regard to the effects of neutron flux on embrittlement of RPV steel at low temperatures of about 50–150°C corresponding to the operating temperature of reactor support structures [3,4,12–14]. All these works reported a negligible effect of neutron flux on embrittlement of RPV steels, except for the case of HFIR surveillance testing. Experimental characterizations of effects of neutron flux on embrittlement, which result in the contrary between at low temperature and at high temperature, may be consistent with theoretical considerations suggesting that, at low temperature, the primary radiation damage processes may be different from those at high temperature [15].

In most experimental studies, however, neutron irradiation has been conducted at a temperature of about 290°C on the steels with relatively higher copper content of more than approximately 0.1 wt%. Furthermore, although neutron irradiation at different irradiation positions of the same reactor must be more advantageous to determine the neutron flux effects because of the capability of minimizing accompanying changes in the effects of neutron energy spectrum, most of the studies with regard to the neutron flux effects have not been based on irradiation in the same reactor. Thus, the effects of neutron flux on embrittlement of low copper steels irradiated at low temperature have not been sufficiently worked out.

The objective of this study is to examine experimentally the effect of neutron flux as an irradiation variable on embrittlement of RPV steels with two different low copper contents. Neutron irradiation at low temperatures in the range from 50°C to 150°C in a test reactor was made to three different neutron fluences up to $\sim 7 \times 10^{22}$ n m^{-2} at the same irradiation positions of neutron fluxes ranging from $\sim 6 \times 10^{14}$ to $\sim 8 \times 10^{16}$ n m^{-2} s^{-1} for reducing an intervention of both irradiation temperature and neutron spectrum effects.

2. Experimental procedure

2.1. Specimen materials

Commercial nuclear RPV steels of A533B class 1 plate materials having two different copper contents of 0.03 wt% (referred as Low Cu steel) and 0.14 wt% (referred as High Cu steel) were used for this study. The High Cu steel also contains other impurity elements like silicon, phosphorus, sulfur, and so on, which are higher than the Low Cu steel does. Table 1 shows chemical compositions of the steels. The steels had been quenched, tempered and subsequently stress-relief heat-treated prior to being provided for this study. The thickness and the heat treatment conditions of the original steel blocks were listed in Table 2. Miniature Charpy V-notch impact specimens were machined in the longitudinal–transverse direction 35 mm deep in the inner portion of the steel block. Each V-notch was cut in the transverse direction and along the thickness direction of the block. Fig. 1 shows dimensions of the miniature Charpy V-notch impact specimen. The miniature Charpy specimens were encapsulated with inert gas in three irradiation capsules without instrumentation of neutron fluence dosimeters and thermocouples.

Table 1
Chemical compositions of the pressure vessel steels (wt%)

A533B steel	C	Si	Mn	P	S	Ni	Cr	Cu	Mo	V	Al	As	Sn	Sb	Fe
Low Cu	0.18	0.17	1.49	0.0024	0.002	0.67	0.11	0.03	0.53	<0.003	0.019	0.003	0.003	0.0007	Bal.
High Cu	0.20	0.30	1.34	0.011	0.011	0.58	0.13	0.14	0.53	<0.003	0.016	0.012	0.015	0.0041	Bal.

Table 2
Thickness and heat treatment conditions of the original steel blocks

A533B steel	Thickness (mm)	Quench	Temper	Stress relief
Low Cu	213	855/895°C × 5 h, WQ	610/650°C × 7 h, AC	605/615°C × 16 h, FC
High Cu	150	860/882°C × 5 h, WQ	650/679°C × 4 h, AC	605/630°C × 42 h, FC

WQ: Water Quenched, AC: Air Cooled, FC: Furnace Cooled.

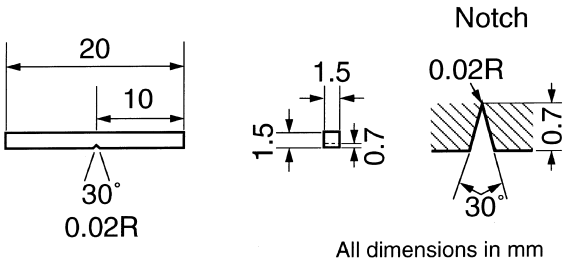

Fig. 1. Dimensions of the miniature Charpy V-notch impact test specimen.

2.2. Neutron irradiation

Neutron irradiation of the capsules was carried out with different neutron fluxes ranging from 5.8×10^{14} to 8.0×10^{16} n m^{-2} s^{-1} ($E > 1$ MeV) to neutron fluences of 5.8×10^{21} to 7.4×10^{22} n m^{-2} ($E > 1$ MeV) in an ambient water temperature of about 50°C in the Japan Materials Testing Reactor (JMTR). Fig. 2 shows a core configuration of the JMTR and the three loading positions of the capsules. The figure also schematically illustrates procedures for drawing out irradiated specimens. Three irradiation capsules, each of which consists of four sub-capsules, were loaded in three different irradiation positions: O-1, K-15 and G-12. Either a part or a whole of the irradiated specimens in the capsule was drawn out in sequence when each desired level of neutron fluences was reached. This was because all the capsules had been designed such that parts of the irradiated specimens could be drawn out without removal of the whole of the capsule. All the capsules were irradiated at different neutron fluxes to the desired neutron fluence levels.

Neutron irradiation conditions of each capsule are summarized in Table 3. Neutron fluxes and neutron energy spectra were calculated with a transport computer code, ANISN-JR [16], and a Monte Carlo computer code, MCNP [17], considering neutron attenuation in the irradiation capsules, because neutron fluences were not measured in the irradiation capsules. The maximum error in calculated neutron flux is estimated to be within 30% [18]. Also, the irradiation temperatures of all the specimens were estimated to be in the range of about 50–150°C taking account of gamma heating using a one-dimensional heat transfer computer code designated GENGTC [19]. The estimated temperatures in Table 3 would be slightly higher than the actual values because we assumed that the specimens are located in a group at the center of the capsule, which means that the amount of heat removal by coolant is less than the actual amount, instead of strictly modeling the configuration of the capsule shown in Fig. 2. The errors of the temperatures are estimated to be within several percents basing on a work by Nomura et al. [20]. Neutron-induced displacement dose and dose rate termed as displacements per atom (dpa) were calculated with all neutron energies using a radiation damage calculation code, SPECTER [21], in order to facilitate comparing results from irradiation facilities having different profiles of neutron energy spectrum.

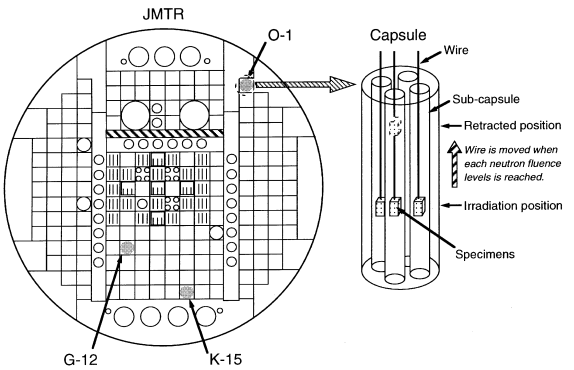

Fig. 2. A core configuration of the Japan Materials Testing Reactor and the three loading positions of the capsules: O-1, K-15 and G-12, and the schematic illustration of irradiated specimen withdrawal.

Fig. 3 indicates a matrix of the irradiation conditions depicting the relationships of neutron fluences versus neutron fluxes. These conditions were devised in such a way as the effect of neutron flux could be studied for three different neutron fluences between $\sim 6 \times 10^{21}$ and $\sim 7 \times 10^{22}$ n m^{-2} ($E > 1$ MeV). Fig. 4 presents typical neutron energy spectra for the three irradiation positions: O-1, K-15 and G-12. The effects of neutron energy spectrum on radiation embrittlement should be neglected since neutron energy spectra at the positions of O-1 and K-15, where neutron fluxes are below $\sim 7 \times 10^{15}$ n m^{-2} s^{-1}, are quite similar to each other and the spectrum at the position of G-12, corresponding to the highest neutron flux level of $\sim 8 \times 10^{16}$ n m^{-2} s^{-1}, is almost similar to those of the other two positions.

2.3. Charpy impact testing

The irradiated miniature Charpy specimens were tested with an instrumented Charpy impact test machine, which was electrically driven with the hydraulic mechanism. The machine utilizes an anvil with a test location in the cryostat and a movable striker. The details of the testing machine and test procedures had been presented elsewhere [22]. The length of the span for the test was adjusted to be 12.5 mm. Control of the test temperature for each test was achieved in the cryostat filled with an appropriate liquid heat-conductive medium. The liquid media used was a mixture of liquid nitrogen and isopentane for temperatures from −120°C up to room temperature, and a silicone oil above room

Table 3
Neutron irradiation conditions estimated using various calculation codes

Irradiation position	Irradiation temperature (°C)	Neutron fluence (n m^{-2})		Neutron flux (n $m^{-2}s^{-1}$)		Thermal-to-fast neutron flux ratio	Displacement [a]	
		Fast ($E > 1$ MeV)	Thermal ($E < 0.683$ eV)	Fast ($E > 1$ MeV)	Thermal ($E < 0.683$ eV)		Dose (mdpa)	Dose rate ($\times 10^{-6}$ mdpa s^{-1})
O-1	52	5.8×10^{21}	2.1×10^{23}	6.2×10^{14}	2.2×10^{16}	36	1.1	0.11
		1.2×10^{22}	4.4×10^{23}	5.8×10^{14}	2.2×10^{16}	38	2.2	0.11
K-15	60	5.9×10^{21}	2.2×10^{23}	6.2×10^{15}	2.3×10^{17}	37	1.1	1.2
		1.4×10^{22}	5.2×10^{23}	7.5×10^{15}	2.8×10^{17}	37	2.7	1.4
		4.4×10^{22}	1.6×10^{24}	7.3×10^{15}	2.7×10^{17}	37	8.3	1.4
G-12	146	7.4×10^{22}	1.4×10^{24}	8.0×10^{16}	1.5×10^{18}	18	12	13

[a] Calculated with all neutron energies.

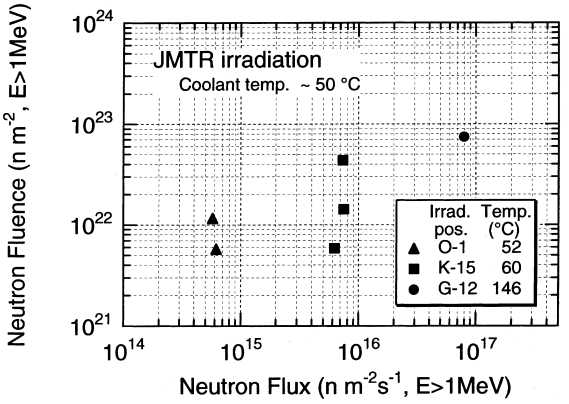

Fig. 3. A matrix of the irradiation conditions depicting relationships of neutron fluences versus neutron fluxes.

temperature. Each specimen was kept at the test temperature for five minutes prior to testing to ensure temperature stabilization.

Data, consisting of the impact load and crosshead displacement with time, from each test were recorded on a digital storagescope and then transferred to a personal computer for storage and analysis. A velocity of the crosshead at an impact was measured on the digital storagescope and found to be 4.6 m s^{-1}.

After each Charpy impact test, observations of the fracture surface of the Low Cu steel specimens were performed with a scanning electron microscope (SEM) to examine fracture appearances and the amount of lateral expansion at the compression side of specimens.

3. Results

3.1. Absorbed energy

An example of the instrumented Charpy impact test data consisting of impact load–time and crosshead displacement–time is shown in Fig. 5. An absorbed energy expressed as the shaded area S in the figure for each specimen was calculated with the following equation:

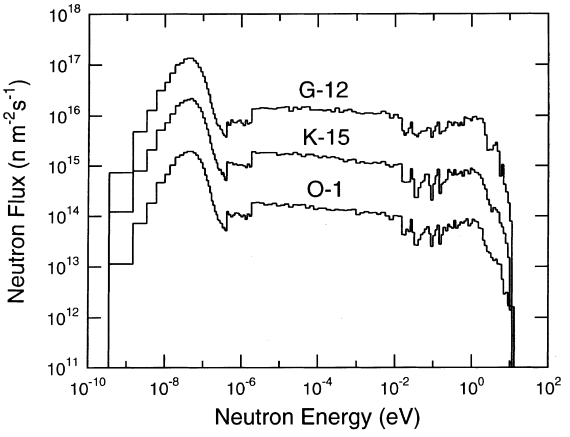

Fig. 4. Typical neutron energy spectra for irradiation positions of O-1, K-15 and G-12.

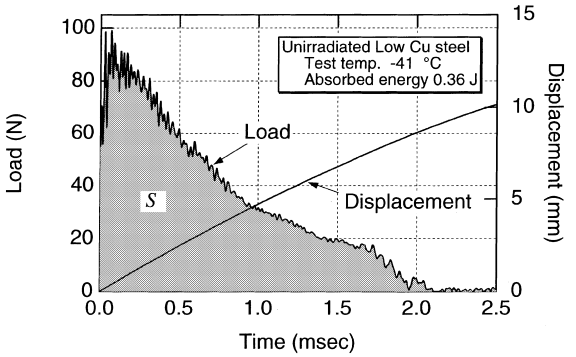

Fig. 5. An example of the instrumented Charpy impact test data consisting of impact load–time and crosshead displacement–time.

$$E = V_0 \int_0^t P(\tau)\, \mathrm{d}\tau, \tag{1}$$

where E is the absorbed energy, V_0 the crosshead speed, $P(\tau)$ the load as a function of time, and t the elapsed time after the test started.

The Charpy impact test results of the miniature Charpy specimens unirradiated and irradiated with various neutron fluences and fluxes are represented in Fig. 6, as a function of test temperature. All the ductile-to-brittle transition curves were drawn with the curve fitting expression in a hyperbolic tangent function of

$$E = C_0 + C_1 \tanh\{C_2(T - C_3)\}, \tag{2}$$

where E is the absorbed energy, T the test temperature, and C_0–C_3 are the fitting coefficients. To determine numerical values of the coefficients for the irradiated specimens, the lower shelf energy (LSE) of the unirradiated specimens was expediently used to estimate the LSE of the irradiated specimens because there was not enough of the absorbed energy data of the irradiated specimens at the LSE level. The upper shelf energy (USE) level was derived from the average data in the USE region of the unirradiated and irradiated specimens. It is found from the figure that the transition curves for the irradiated steels are well fitted although a scatter of the data for the irradiated specimens is larger than that for the unirradiated ones.

The ductile-to-brittle transition temperature (DBTT) was defined as a half of the USE. Table 4 summarizes the results of the USE and DBTT for unirradiated and irradiated specimens. As can be seen from the table, the DBTT obviously increases and the USE slightly decreases with neutron fluence for both Low Cu steel and High Cu steel, indicating that embrittlement of both steels depends on neutron fluence levels. The irradiation-induced increments in DBTT (ΔDBTT at 1/2 USE) of

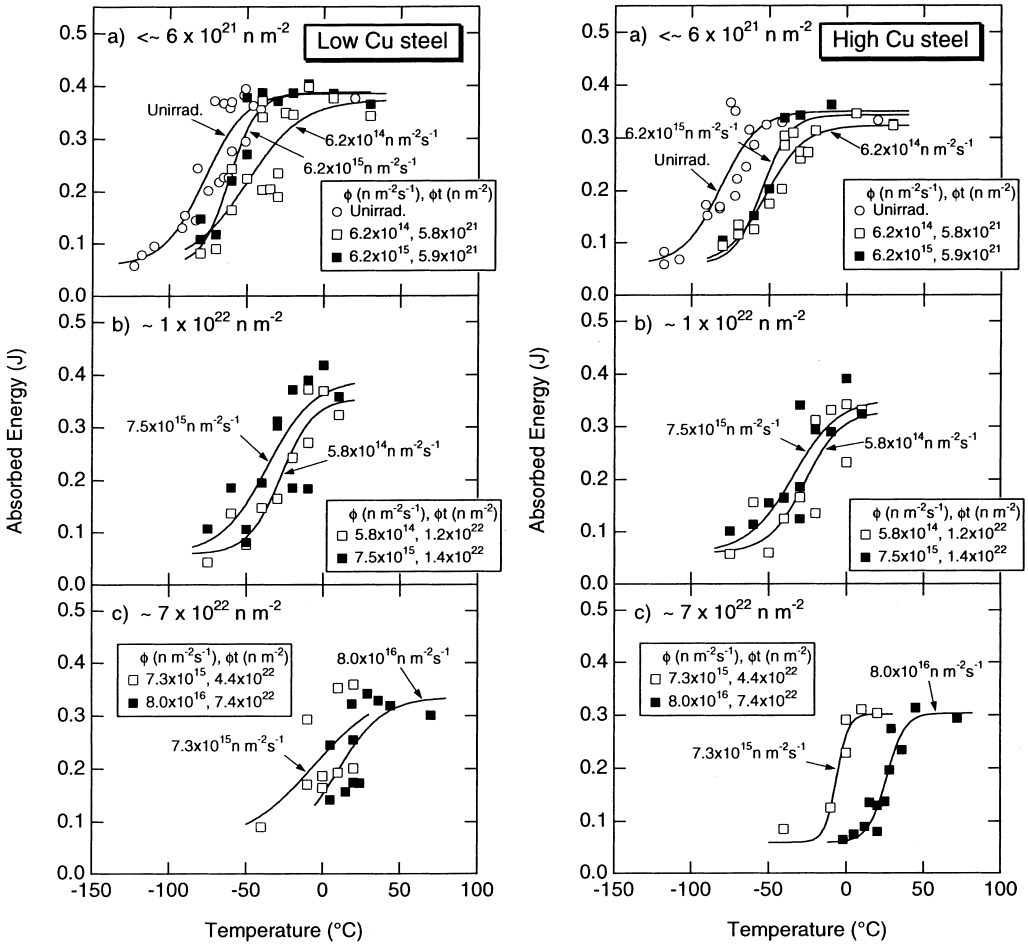

Fig. 6. The Charpy impact test results of the miniature Charpy specimens unirradiated and irradiated with various neutron fluences and fluxes.

Table 4
A summary of the results of the USE and DBTT for unirradiated and irradiated specimens

A533B steel	Neutron fluence (n m^{-2}, $E > 1$ MeV)	Neutron flux (n $m^{-2}s^{-1}$, $E > 1$ MeV)	USE (J)	ΔUSE (J)	DBTT at 1/2 USE (°C)	ΔDBTT at 1/2 USE(°C)
Low Cu	Unirrad.	Unirrad.	0.39	0.00	−82	0
	5.8×10^{21}	6.2×10^{14}	0.37	−0.02	−57	25
	5.9×10^{21}	6.2×10^{15}	0.39	0.00	−65	17
	1.2×10^{22}	5.8×10^{14}	0.36	−0.03	−32	50
	1.4×10^{22}	7.5×10^{15}	0.39	0.00	−42	40
	4.4×10^{22}	7.3×10^{15}	0.36	−0.03	−14	68
	7.4×10^{22}	8.0×10^{16}	0.34	−0.05	4	86
High Cu	Unirrad.	Unirrad.	0.35	0.00	−87	0
	5.8×10^{21}	6.2×10^{14}	0.32	−0.03	−58	29
	5.9×10^{21}	6.2×10^{15}	0.34	−0.01	−59	28
	1.2×10^{22}	5.8×10^{14}	0.33	−0.02	−32	55
	1.4×10^{22}	7.5×10^{15}	0.35	0.00	−40	46
	4.4×10^{22}	7.3×10^{15}	0.30	−0.05	−8	79
	7.4×10^{22}	8.0×10^{16}	0.30	−0.05	23	110

the High Cu steel are larger than those for the Low Cu steel, although the difference in the irradiation-induced increments in USE (ΔUSE) is unclear between both steels.

Fig. 7 shows an increase in DBTT of both Low Cu steel and High Cu steel as a function of neutron fluence for three different neutron flux levels of $\sim 6 \times 10^{14}$, $\sim 7 \times 10^{15}$, and $\sim 8 \times 10^{16}$ n m^{-2} s^{-1}. For both steels, the lowest neutron flux level ($\sim 6 \times 10^{14}$ n m^{-2} s^{-1}) caused a larger embrittlement than the intermediate flux level ($\sim 7 \times 10^{15}$ n m^{-2} s^{-1}) did in the lower neutron fluence range of $\sim 6 \times 10^{21}$ to $\sim 1 \times 10^{22}$ n m^{-2} . At a neutron fluence of $\sim 1 \times 10^{22}$ n m^{-2}, in particular, ΔDBTTs for the lowest neutron flux level ($\sim 6 \times 10^{14}$ n m^{-2} s^{-1}) was a maximum of about 10°C larger than that for the intermediate neutron flux level ($\sim 7 \times 10^{15}$ n m^{-2} s^{-1}), and the neutron flux effect for Low Cu steel also appears to be slightly larger than that for High Cu steel. At a neutron fluence of $\sim 7 \times 10^{22}$ n m^{-2}, to the contrary, ΔDBTT for the intermediate flux level ($\sim 7 \times 10^{15}$ n m^{-2} s^{-1}) was agreed well with that for the highest flux of $\sim 8 \times 10^{16}$ n m^{-2} s^{-1} when the trend at the fluence was extrapolated to the higher neutron fluence for both steels. This may be a consequence of negligible neutron flux effect due to the saturation of embrittlement at the higher neutron fluence level.

The differences in ΔDBTT between the High Cu steel and Low Cu steel are plotted in Fig. 8 against neutron fluence for three different neutron flux levels. Apparently the ΔDBTT of the High Cu steel is larger than that for the Low Cu steel at all the neutron fluence levels. This can be due to compositional effect on embrittlement. It should be noted that the compositional effect significantly increases with increasing neutron fluences, and is always smaller for the lowest neutron flux level than for the intermediate neutron flux level in the lower neutron fluence range of $\sim 6 \times 10^{21}$ to $\sim 1 \times 10^{22}$ n m^{-2}.

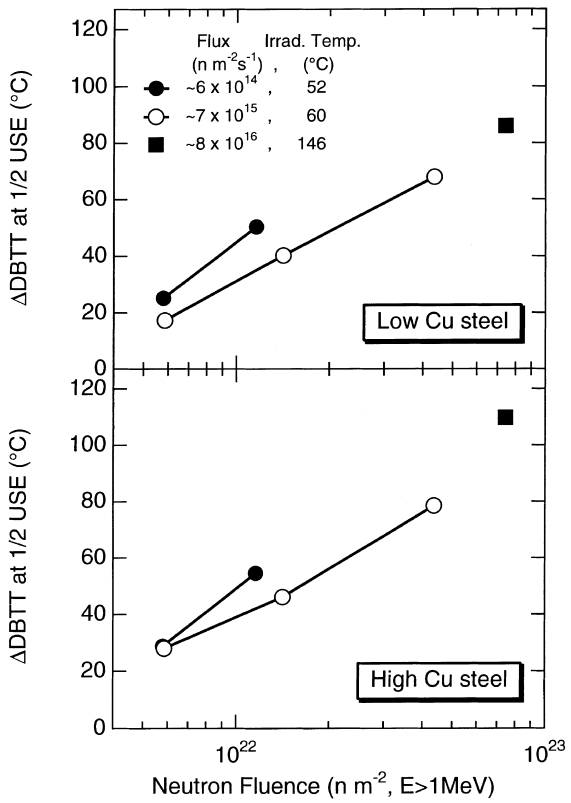

Fig. 7. An increase in ductile-to-brittle transition temperature both Low Cu steel and High Cu steel as a function of neutron fluence for three different neutron flux levels of $\sim 6 \times 10^{14}$, $\sim 7 \times 10^{15}$, and $\sim 8 \times 10^{16}$ n m^{-2} s^{-1}.

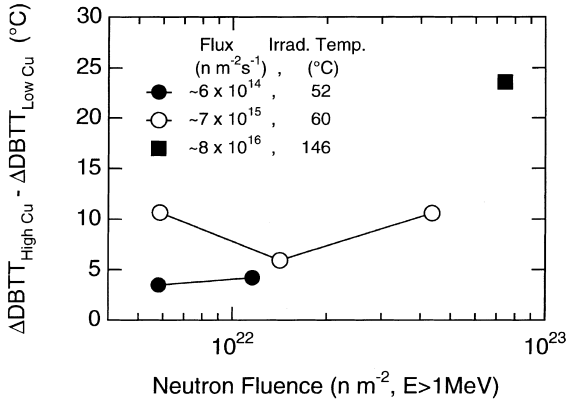

Fig. 8. A difference in ductile-to-brittle transition temperature increase between Low Cu steel and High Cu steel as a function of neutron fluence for three different neutron flux levels.

3.2. Fracture surface observation

Observations of fracture surfaces of the Charpy impact specimens in the LSE, transition and USE regions were made for the Low Cu steel unirradiated and irradiated at various fluxes to neutron fluences up to 7.4×10^{22} n m^{-2}. The unirradiated specimens in the LSE region fractured completely in a brittle manner, whereas these in the transition region did in such ways as the brittle fracture concentrated in the center and the ductile failure surrounded the periphery. In the USE region the fracture surface of the unirradiated specimen was characteristic of a ductile dimple failure mode. These trends of the fracture mode were unchanged for the irradiated specimens as well. Typical fracture surfaces in the LSE, transition and USE regions of the Low Cu steel irradiated at a neutron flux of 5.8×10^{14} n m^{-2} s^{-1} to a neutron fluence of 1.2×10^{22} n m^{-2} are presented in Fig. 9. The features of the miniature Charpy specimen in this study were the same as those for the full size Charpy specimen, implying that the effect of specimen size on the fracture surface was negligible.

3.3. Lateral expansion and percent brittle fracture

Lateral expansion and brittle fracture fraction were derived from the fracture surface observation of the specimen. The results were that the lateral expansion and the absorbed energy increased with test temperature. The behavior of the temperature dependent lateral expansion and the absorbed energy were quite consistent with each other. On the contrary, the brittle fracture fraction decreased with increasing test temperature.

This tendency is also reasonable in terms of the ductile-to-brittle transition behavior. From the above results, again, we can define another DBTT in such two different ways as the temperature corresponding to a lateral expansion of 0.13 mm and a brittle fracture

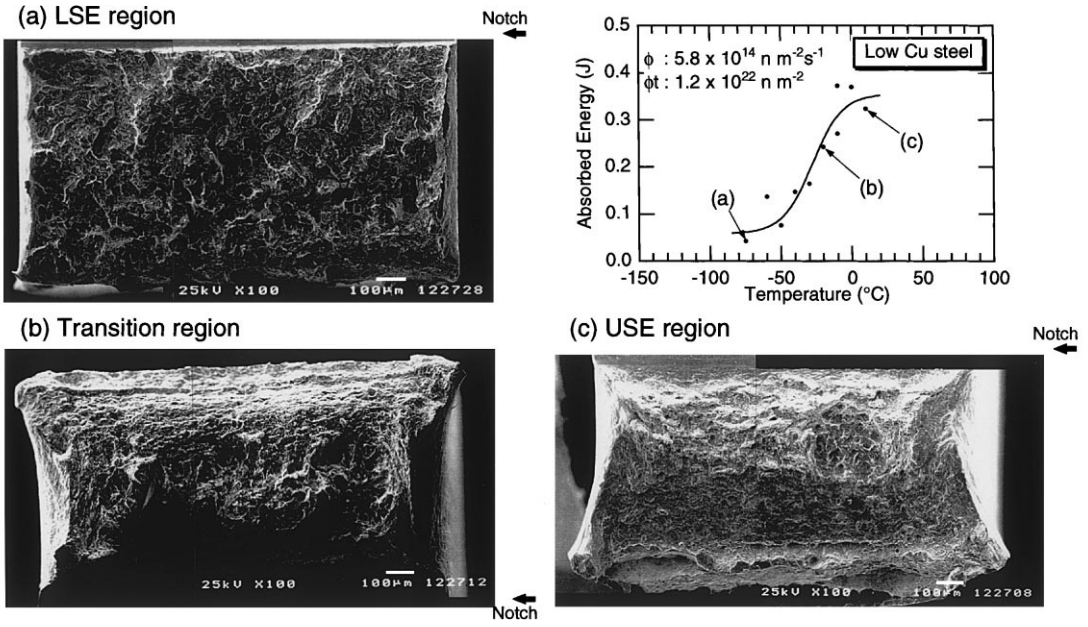

Fig. 9. Typical fracture surfaces in the LSE, transition and USE regions of the Low Cu steel irradiated at a neutron flux of 5.8×10^{14} n m^{-2} s^{-1} to a neutron fluence of 1.2×10^{22} n m^{-2}.

fraction of 50% by interpolating the data of the lateral expansion and the percent brittle fracture. The lateral expansion of 0.13 mm was determined on the assumption that the ratio of the lateral expansion to the width of the specimen unchanges between the miniature and full size Charpy specimen and that the lateral expansion of 0.89 mm (5 mils) generally is used to evaluate a transition temperature for the full size Charpy specimen. The values of ΔDBTT at 50% brittle fracture and at 0.13 mm lateral expansion of the Low Cu steel are plotted in Fig. 10, as a function of neutron fluence for each neutron flux. It is seen that the DBTT deduced from the fracture surface observation increased with neutron fluence, that in the lower neutron fluence range the lowest neutron flux level induced a larger embrittlement than the intermediate flux level did, and that in the higher neutron fluence the neutron flux effect on embrittlement does not matter. It is apparent from Figs. 7 and 10 that the DBTT agrees very well between the two different definitions based on the Charpy impact testing and the fracture surface observation.

It is surmised from the above that a close relation must exist among absorbed energy, lateral expansion and brittle fracture fraction. Fig. 11 depicts relationships of lateral expansion, and of brittle fracture fraction versus absorbed energy for the Low Cu steel specimens tested in this study. Again, it is manifested that correlations between lateral expansion, brittle fracture fraction and absorbed energy are very well, suggesting that correlations found on the full size Charpy V-notch impact specimen has been recognized on the miniature Charpy V-notch impact specimens as well and that the miniature Charpy V-notch impact specimen may also be useful.

4. Discussion

The results of this study using the miniature Charpy V-notch impact specimens showed that embrittlement of the RPV steel at the lowest neutron flux level was larger than that for the intermediate neutron flux level in the neutron fluence range of $\sim 6 \times 10^{21}$ to $\sim 1 \times 10^{22}$ n m^{-2}

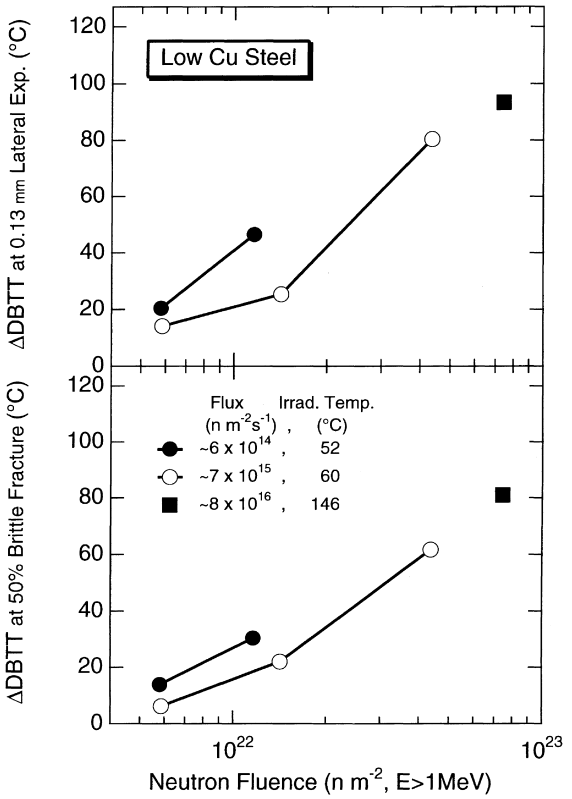

Fig. 10. An increase in ductile-to-brittle transition temperature at 50% brittle fracture and at 0.13 mm lateral expansion of the Low Cu steel as a function of neutron fluence for the different neutron flux levels.

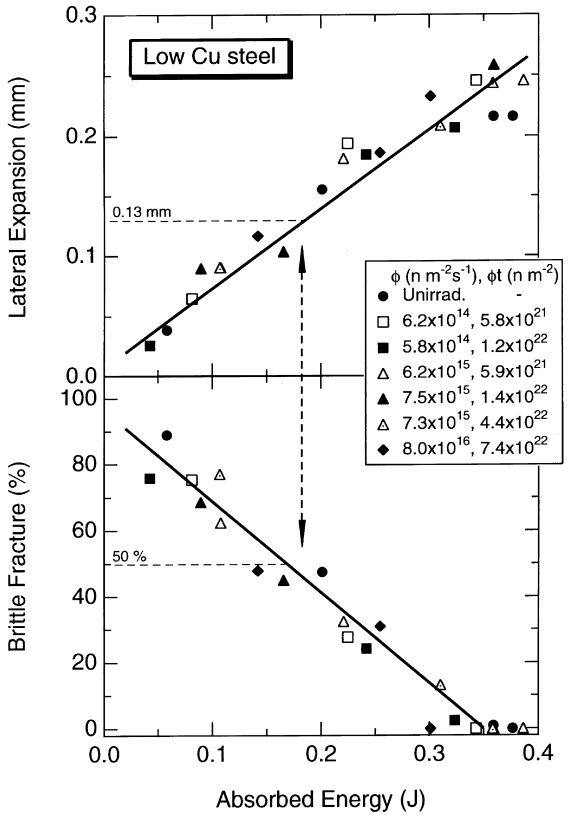

Fig. 11. Relationships of lateral expansion, and of brittle fracture fraction versus absorbed energy for the Low Cu steel.

at irradiation temperatures below 60°C whereas it was almost unchanged between the intermediate and highest neutron flux levels in the higher fluence level of $\sim 7 \times 10^{22}$ n m^{-2} at irradiation temperatures below 150°C, as shown in Fig. 7. The neutron flux effect for the Low Cu steel trended to be slightly larger than that for the High Cu steel. Since the results were based on the data from the miniature Charpy specimens, they must be carefully discussed and assessed. We therefore made an attempt to estimate data for the full size Charpy specimens from those obtained for the miniature Charpy specimens in this study first and then evaluated the results in more quantitative manner than those reported in the literature.

4.1. Estimation of ΔDBTT for the full size Charpy specimen

Louden et al. [23] showed that the increases in DBTT for the full size V-notch Charpy impact specimens could be predicted from those for the half and third size V-notch Charpy impact specimens by proposing a normalization factor for the DBTT based on the assumption that increases in the normalized DBTT with heat treatment and neutron irradiation of the specimen is independent of the size and notch geometry. Furthermore, Kayano et al. [24] developed and proposed a normalization factor to estimate DBTT for the full size V-notch Charpy impact specimens from that for the miniature V-notch Charpy impact specimens having cross sections of 1.0×1.0 and 1.5×1.5 mm^2 for several kinds of neutron irradiated ferritic steels. The equation of correlating between $\Delta DBTT_{full}$ and $\Delta DBTT_{mini}$, which are irradiation-induced increments in $DBTT_{full}$ and $DBTT_{mini}$ for the full size and miniature Charpy specimens, respectively, used in the study of Kayano et al., was given by

$$\Delta DBTT_{full} = \frac{NF_{full}}{NF_{mini}} \cdot \Delta DBTT_{mini} = \sqrt{\frac{(K_t Q)_{full}}{(K_t Q)_{mini}}} \cdot \Delta DBTT_{mini}, \quad (3)$$

where NF_{full} and NF_{mini} are normalization factors for the full size and miniature Charpy specimens, respectively. K_t is the elastic stress concentration coefficient defined by Neuber [25] and Q is given approximately by an equation of $Q = 1 - \theta/2 + \pi/2$ (θ: the notch angle) [26].

Table 5 lists the numerical values of each parameter in the above correlation Eq. (3) for the geometry of the miniature Charpy specimen used in this study, and of the standard full size Charpy specimen. Eq. (3) was eventually expressed as follows:

$$\Delta DBTT_{full} = 0.92 \cdot \Delta DBTT_{mini}. \quad (4)$$

Table 5
Geometrical parameters for the full size and miniature Charpy specimens

Size	θ (rad)	K_t	Q
Full	0.785	4.81	2.18
Mini	0.524	5.34	2.31

This correlation equation was used to estimate values of ΔDBTT for the full size Charpy V-notch impact test specimens from those of the miniature Charpy specimens of this study.

The estimated values of $\Delta DBTT_{full}$ from the miniature Charpy specimen data are plotted in Fig. 12 (a) and (b) as a function of neutron fluence and displacement dose (dpa), together with those from the HFIR surveillance testing, which was analyzed by Remec et al. [5], the accelerated irradiation in the Oak Ridge Research Reactor (ORR) [4], and the Shippingport neutron shield

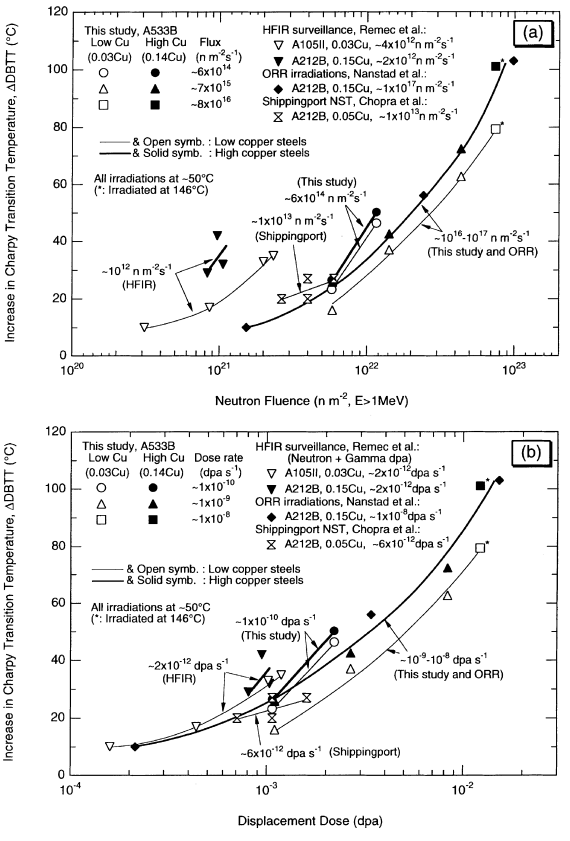

Fig. 12. Comparison of the increase in Charpy transition temperature estimated from the miniature Charpy specimen with data from the HFIR surveillance testing [5], the ORR irradiations [4] and the Shippingport NST [12] as a function of fast neutron fluence (a) and dpa (b). Both neutron-induced and gamma-induced displacements only for the HFIR surveillance data are take into account in (b).

tank (NST) [12]. It is obvious from Fig. 12 (a) that our High Cu steel data for the higher neutron flux range of $\sim 7 \times 10^{15}$ to $\sim 8 \times 10^{16}$ n m^{-2} s^{-1} agree well with those for the test reactor irradiation in the ORR.

However, the HFIR surveillance testing data cannot be compared with our data directly because the accelerated embrittlement of those data was due to gamma-induced displacements, as pointed out by Remec et al. [5]. Therefore, we made a comparison further based on displacement dose, as shown in Fig. 12 (b). In this figure both neutron-induced and gamma-induced displacements only for the HFIR surveillance data, which were analyzed by Remec et al. [5], are taken into consideration. Our High Cu steel data for higher displacement dose rate range of $\sim 1 \times 10^{-9}$ to $\sim 1 \times 10^{-8}$ dpa s^{-1} are in good agreement with those for ORR irradiations as the comparison is made based on fast neutron fluences. Also, our Low Cu steel and High Cu steel data for the lowest displacement dose rate of $\sim 1 \times 10^{-10}$ dpa s^{-1} are consistent with those for the low (0.03 wt%) and high (0.15 wt%) copper materials, respectively, in the HFIR surveillance testing.

4.2. Neutron flux effect

It is apparent from this work that among three different neutron flux levels of $\sim 6 \times 10^{14}$, $\sim 7 \times 10^{15}$, and $\sim 8 \times 10^{16}$ n m^{-2} s^{-1}, the lowest neutron flux level tended to induce a larger increase in DBTT than the intermediate and highest rate did for both Low Cu steel and High Cu steel in the lower neutron fluence range of $\sim 6 \times 10^{21}$ to $\sim 1 \times 10^{22}$ n m^{-2}. Also, the comparisons made in Fig. 12 would allow to discuss the neutron flux or the displacement dose rate effect on embrittlement of RPV steels under the low temperature neutron irradiation around 50°C, together with those for other facilities, since our data converted to the increases in DBTT for the full size Charpy specimens from those for the miniature Charpy specimens are almost consistent with the data from other facilities.

Fig. 13 (a) and (b) shows normalized ΔDBTTs as a function of neutron flux and displacement dose rate, defined as ΔDBTT divided by a square root of the neutron fluence and displacement dose, respectively, for the data from this work, the HFIR surveillance testing [5], the ORR irradiations [4] and the Shippingport NST [12]. The normalized ΔDBTTs tend to increase with decreasing neutron flux for the results of this work as well as of the other irradiation facilities published in literature, as shown in Fig. 13 (a). It should be noted that the HFIR surveillance testing data revealed more significant effect of neutron flux than our results did, due to the fact that the accelerated embrittlement of the HFIR surveillance testing data could be explain in terms of uncounted dpa induced by gamma rays as Remec et al. [5] reported.

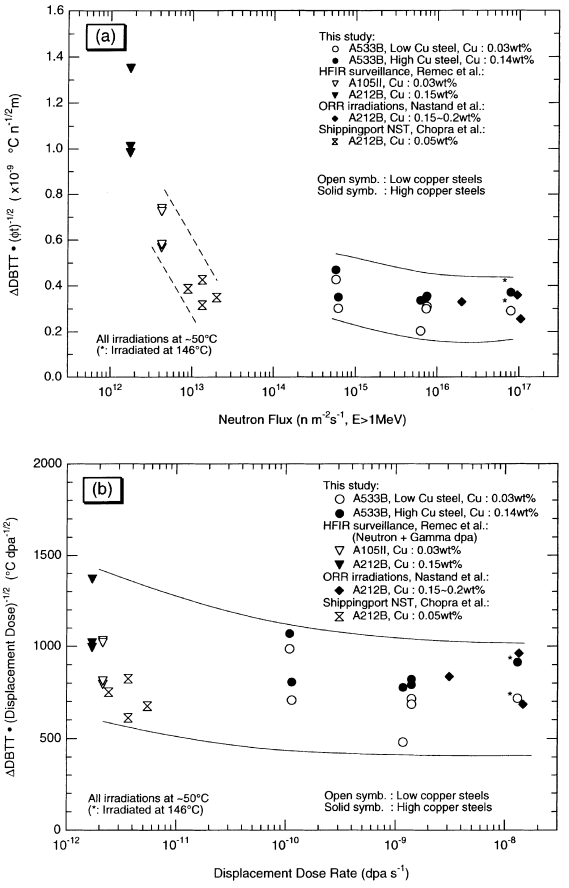

Fig. 13. Normalized increases in ductile-to-brittle transition temperature as a function of neutron flux (a) and displacement dose rate (b), defined as increase in ductile-to-brittle transition temperature divided by a square root of the neutron fluence and the displacement dose, respectively, for the data from this work, the HFIR surveillance testing [5], ORR irradiations [4] and the Shippingport NST [12]. Both neutron-induced and gamma-induced displacements only for the HFIR surveillance data are taken into account in (b).

Actually, as shown in Fig. 13 (b), the displacement dose rate effect for the HFIR data appears to be negligible provided that the gamma-induced displacement are taken account of in the data. The normalized ΔDBTTs as a whole in Fig. 13 (b), however, tend to slightly increase with decreasing displacement dose rate. This suggests that there is a weak dependence of displacement dose rate not only for our data but also for the data by the other facilities.

On the contrary to the above, Barton et al. [14] reported a negligible neutron flux effect on hardening of mild steels irradiated at temperatures of 100 to 350°C in the neutron flux range of about 3×10^{15} to 3×10^{17} n m^{-2} s^{-1} for a neutron fluence of about 3×10^{21} n m^{-2}, and also Odette et al. [13] indicated

that the hardening of steels with various copper contents irradiated at 60°C up to a fast fluence of about 3×10^{22} n m^{-2} in the test reactor was independent of neutron flux ranging from 2×10^{13} to 5×10^{18} n m^{-2} s^{-1}. The data reported by Barton et al. and Odette et al. are based on yield stress by tensile testing, while all data shown in Fig. 13 are based on absorbed energy by Charpy impact testing. An inconsistency in the neutron flux (or the displacement dose rate) effect between the data shown in Fig. 13 and the data reported by Barton et al. and Odette et al. can be ascribable to the different experimental test. In general, yield stress by tensile testing have been correlated with absorbed energy by Charpy impact testing because embrittlement of RPV steels manifested by a shift in the transition temperature delineating ductile and brittle cleavage fracture regimes is primarily caused by yield stress increases produced by the fine scale microstructural features that are formed under irradiation. However, Nagasaka et al. [27] have reported that the neutron flux effect in a ferritic steel (Fe–Cr–W) irradiated at low temperature below 100°C did not emerge as the change of yield stress, but as those of elongation and absorbed energy by tensile testing. This suggests that yield stress by tensile testing is not necessarily correlated with absorbed energy by Charpy impact testing.

Some theoretical models have been developed to predict embrittlement of RPV steels based on the assumption that the embrittlement are primary caused by point defect clusters and copper-rich precipitates. Stoller [28,29] calculated the fraction of matrix recombination of point defect in temperatures of 60°C and 288°C, and predicted the displacement dose rate effect on radiation-induced increments in yield strength due to point defect clusters based on a dislocation barrier model taking account of the Orowan-looping mechanism. The results showed that the fraction of interstitial point defects avoiding matrix recombination decreased with increasing the displacement dose rate while the increments in yield strength increased with increasing the displacement dose rate at both irradiation temperatures of 60°C and 288°C. The predicted results of the increments in yield strength are inconsistent with the results from our data and other facilities shown in Fig. 13 (b) if only it is valid that the radiation-induced increments in Charpy transition temperature is in proportion to that of yield strength. The prediction of radiation-induced hardening based only on the population of point defect clusters may result in the inconsistency with the trend obtained from several experiments because the population of point defect clusters is dominated by the clusters formed in cascades, which decrease with decreasing displacement dose rate [15]. Therefore, a theoretical model consistent with the experimental results will require other possible mechanisms besides the population of point defect clusters.

4.3. Compositional effect

The compositional effect on radiation-induced embrittlement of steels used in this work was observed. The effect, which significantly increased with increasing neutron fluences and trended to increase with increasing neutron fluxes, can be caused by residual impurity elements like copper, silicon, phosphorus, sulfur and so on, in the Low Cu steel and High Cu steel.

It is widely known that embrittlement of RPV steels irradiated at 288°C depends on residual impurity contents. There are lots of works manifesting that copper impurity, in particular, can cause radiation-induced embrittlement in such a way as the fine copper-rich precipitates are formed during irradiation. However, at a low irradiation temperature of about 50°C, several works indicated that there is an effect of copper on embrittlement in higher neutron fluence levels, but not in low neutron fluence levels. Farrell et al. [15], for example, reported that in iron model alloys containing copper and nickel, there was no effect of the alloying elements on radiation strengthening up to a neutron fluence of 9.4×10^{21} n m^{-2}, and the strengthening increased with neutron fluence at higher neutron fluences, while, in some steels, a copper and nickel effect emerged at a neutron fluence of 1.9×10^{23} n m^{-2}. Also, Odette and co-workers [13], who carried out experiments with model iron and steel alloys of copper level of less than 0.8 wt% and nickel level of less than 1.6 wt% irradiated at a neutron fluence of 3×10^{22} n m^{-2}, indicated that there was some evidences of moderate copper effects at low nickel contents and nickel effects at low copper contents while copper effects at high nickel contents and nickel effects at high copper contents are negligibly weak. These results appear to be quite consistent with our data. Although it is known that the hardening at higher irradiation temperatures is due to radiation-induced precipitates containing impurities like copper, it is confirmed that the hardening at low irradiation temperatures is not due to radiation-induced precipitates but due to very small microstructural features, which can not be identified by transmission electron microscope but by small angle neutron scattering measurements [13]. This means that the dominant mechanism of embrittlement at low irradiation temperatures is different from that at higher irradiation temperatures. Since it is suggested that the primary effect of copper and nickel at low irradiation temperatures may be to promote more point defect clusters because at low irradiation temperatures the point defects trapped at solute atoms are more stable than at higher temperatures [15], compositional effects at low irradiation temperatures may be caused by the difference in the population of point defect clusters, which controls radiation-induced hardening and embrittlement by combining with residual impurities like copper and nickel. However, further investigations are

required to clarify the role of the point defect that induces compositional effects as well as neutron flux effects on the radiation-induced hardening and embrittlement of RPV steels.

5. Conclusions

The effect of neutron flux on commercial reactor pressure vessel steels having two different copper contents of 0.03 wt% (referred as low copper steel) and 0.14 wt% (referred as high copper steel), irradiated at different irradiation positions of the same test reactor at low temperatures in the range from 50°C to 150°C was investigated by using miniature Charpy V-notch impact test specimens. The neutron fluxes were ranging from $\sim 6 \times 10^{14}$ to $\sim 8 \times 10^{16}$ n m^{-2} s^{-1} ($E > 1$ MeV) and neutron fluences were in the range from $\sim 6 \times 10^{21}$ to $\sim 7 \times 10^{22}$ n m^{-2} ($E > 1$ MeV). The conclusions drawn are as follows.

1. The radiation-induced embrittlement at a low neutron flux level of $\sim 6 \times 10^{14}$ n m^{-2} s^{-1} ($E > 1$ MeV) for both low and high copper steels were greater than those for neutron flux levels of $\sim 7 \times 10^{15}$ n m^{-2} s^{-1}. The neutron flux effect on embrittlement tended to be more pronounced in the lower neutron fluence range of $\sim 6 \times 10^{21}$ to $\sim 1 \times 10^{22}$ n m^{-2} than in the higher neutron fluence level of $\sim 7 \times 10^{22}$ n m^{-2}, and also to be larger for the low copper steel than for the high copper steel.

2. The displacement dose rate effect on embrittlement of steels irradiated at different irradiation positions of the same reactor in this work was consistent with data obtained from neutron irradiation at different reactors in the literature regarding neutron irradiation at low temperature of about 50°C, indicating that embrittlement tended to slightly increase with decreasing the displacement dose rate.

3. The radiation-induced embrittlement was larger for the high copper steel than for the low copper steel regardless of the neutron fluence and flux. The compositional effect significantly increased with increasing neutron fluences and trended to increase with increasing neutron fluxes. It is suggested that the effect at low irradiation temperature may be caused by the difference in the population of point defect clusters by combining with residual impurity elements like copper, nickel, silicon, sulfur and so on.

Acknowledgements

The authors thank Mr M. Yamazaki for his assistance in this experimental works at the hot laboratory of Tohoku University, Mr M. Kusuhashi of the Japan Steel Works, Ltd., for his providing steels. We also thank Mr Y. Nagao and Mr T. Sagawa of Japan Atomic Energy Research Institute for their estimation of irradiation conditions, Dr L.R. Greenwood of Pacific Northwest Laboratory for his offer of SPECTER computer code to calculate the displacement dose. Thanks are extended to Dr N. Soneda for his comments and suggestions while reviewing this paper.

References

[1] Radiation Embrittlement of Reactor Vessel Materials, US Nuclear Regulatory Commission Regulatory Guide 1.99, Revision 2, May 1988.
[2] Surveillance Tests of Structural Materials for Nuclear Reactors, Japanese Electric Associations, Japanese Electric Association Codes (JEAC) 4201-1991, 1991, in Japanese.
[3] R.K. Nanstad, K. Farrell, D.N. Braski, W.R. Corwin, J. Nucl. Mat. 158 (1988) 1.
[4] R.K. Nanstad, S.K. Iskander, A.F. Rowcliffe, W.R. Corwin, G.R. Odette, in: N.H. Packan, R.E. Stoller, A.S. Kumar (Eds.), Proc. 14th Int. Symp. on Effects of Radiation on Materials, vol. II, ASTM-STP 1046 (1990) 5.
[5] I. Remec, J.A. Wang, F.B.K. Kam, K. Farrell, J. Nucl. Mater. 217 (1994) 258.
[6] J.R. Hawthorne and A.L. Hiser, in: N.H. Packan, R.E. Stoller, A.S. Kumar (Eds.), Proc. 14th Int. Symp. on Effects of Radiation on Materials, vol. II, ASTM-STP 1046 (1990) 55.
[7] M. Suzuki, Y. Idei, M. Kizaki, K. Onizawa, in: R.K. Nanstad, M.L. Hamilton, F.A. Garner, A.S. Kumar (Eds.), Proc. 18th Int. Symp. on Effects of Radiation on Materials, ASTM-STP 1325, to be published.
[8] J.A. Wang, in: R.K. Nanstad, M.L. Hamilton, F.A. Garner, A.S. Kumar (Eds.), Proc. 18th Int. Symp. on Effects of Radiation on Materials, ASTM-STP 1325, to be published.
[9] A.D. Amaev, E.A. Krasikov, A.M. Krjukov, P.A. Platonov, E.P. Ryazantsev, M.A. Sokolov, Ya.I. Shtrombakh, in: Proc. The Japanese–Russian Seminar on Integrity Assurance and Irradiation Effects on Reactor Pressure Vessel, Tokyo, Japan, 18–20 May 1993.
[10] D. Pachur, in: D. Kramer, H.R. Brager, J.S. Perrin (Eds.), Proc. 10th Conf. on Effects of Radiation on Materials, ASTM-STP 725 (1981) 5.
[11] M. Suzuki, K. Onizawa, M. Kizaki, in: D.S. Gelles, R.K. Nanstad, A.S. Kumar, E.A. Little (Eds.), Proc. 17th Int. Symp. on Effects of Radiation on Materials, ASTM-STP 1270 (1996) 351.
[12] O.K. Chopra, W.J. Shack, S.T. Rosinski, Radiation embrittlement of the neutron shield tank from the shippingport reactor, Argonne National Laboratory, NUREG/CR-5748, ANL-91/23, SAND91-1993, October 1991.
[13] G.R. Odette, G.E. Lucas, R.D. Klingensmith, R.E. Stoller, in: D.S. Gelles, R.K. Nanstad, A.S. Kumar, E.A. Little (Eds.), Proc. 17th Int. Symp. on Effects of Radiation on Materials, ASTM-STP 1270 (1996) 547.
[14] P.J. Barton, D.R. Harries, I.L. Mogford, J. Iron Steel Inst. 203 (1965) 507.
[15] K. Farrell, S.T. Mahmood, R.E. Stoller, L.K. Mansur, J. Nucl. Mater 210 (1994) 268.

[16] K. Koyama, Y. Taji, T. Minami, T. Tsutsui, T. Ideta, S. Miyasaka, ANISN-JR: A One Dimensional Discrete Ordinates Code for Neutron and Gamma-ray Transport Calculations, Japan Atomic Energy Research Institute, JAERI-M6954 (1977).
[17] J.F. Briesmeister (Ed.), MCNP: A General Monte Carlo N-Particle Transport Code – Ver. 4A, Los Alamos National Laboratory Report LA-12625-M (1993).
[18] Y. Nagao, private communication.
[19] H.C. Roland, GENGTC: A One-Dimensional CEIR Computer Program for Capsule Temperature Calculation in Cylindrical Geometry, Oak Ridge National Laboratory Report ORNL-TM-1942 (1967).
[20] Y. Nomura, H. Someya, H. Ito, Preparation of Functions of Computer Code GENGTC and Improvement for Two-dimensional Heat Transfer Calculations for Irradiation Capsules (in Japanese), Japan Atomic Energy Research Institute, JAERI-M92-163 (1992).
[21] L.R. Greenwood, R.K. Smither, SPECTER: Neutron Damage Calculations for Materials Irradiations, Argonne National Laboratory Report ANL/FPP/TM-197 (1985).
[22] H. Kayano, H. Kurishita, M. Narui, M. Yamazaki, Ann. Chim. Fr. 16 (1991) 309.
[23] B.S. Louden, A.S. Kumar, F.A. Garner, M.L. Hamilton, W.A. Hu, J. Nucl. Mater. 155–157 (1988) 662.
[24] H. Kayano, H. Kurishita, A. Kimura, M. Narui, M. Yamazaki, Y. Suzuki, J. Nucl. Mater. 179–181 (1991) 425.
[25] H. Neuber, Theory of Notch Stresses, 2nd ed., Springer, Berlin, 1958, p. 71.
[26] A.S. Teleman, A.J.R. McEvily, Fracture of Structural Materials, Wiley, New York, 1967.
[27] T. Nagasaka, H. Kayano, T. Shibayama, M. Narui, I. Yoshii, Progress Report of the Oarai Branch IMR Tohoku University (in Japanese), vol. 14, 1996, pp. 57–61.
[28] R.E. Stoller, in: A.S. Kumar, D.S. Gelles, R.K. Nanstad, E.A. Little (Eds.), Proc. 16th Int. Symp. on Effects of Radiation on Materials, ASMT-STP 1175 (1993) 394.
[29] R.E. Stoller, in: D.S. Gelles, R.K. Nanstad, A.S. Kumar, E.A. Little (eds.), Proc. 17th Int. Symp. on Effects of Radiation on Materials, ASTM-STP 1270 (1996) 25.